Contrasting Behaviors of Metal Fullerides $C_{60}Rh_x$ and $C_{60}M_x$ (M = La, Y) in the Metallofullerene Formation by Laser Ablation

Qingyu Kong,[†,§] Jun Zhuang,[‡] Jiong Xu,[‡] Yifeng Shen,[†] Yufen Li,[†,‡] and Li Zhao*[,†,‡]

Department of Physics, Fudan University, Shanghai 200433, China, State Key Laboratory for Advanced Photonic Materials and Devices, Fudan University, Shanghai 200433, China, and Department of Chemistry & Laser Chemistry Institute, Fudan University, Shanghai 200433, China

Ruifang Cai

Department of Chemistry, Fudan University, Shanghai 200433, China

Received: November 25, 2002; In Final Form: February 27, 2003

Contrasting behaviors of Rh with Y(La) in the formation of metallofullerenes by excimer laser ablation of metal fullerides $C_{60}Rh_x$ and $C_{60}M_x$ (M = La, Y) were observed. For Rh, two sequences of rhodium metallofullerenes, $C_{2n}Rh$ and $C_{2n+1}Rh$ with even and odd numbers of carbon atoms, are formed in both the negative and positive ion channels, but for La and Y, only the metallofullerene sequence with even numbers of carbon atoms is formed and only in the positive ion channel. Evidence of the encapsulation of La and Y atoms in fullerene cages forming endohedral fullerenes has been observed, whereas the Rh atom is most probably incorporated into the network of the fullerene cage or pseudo-fullerene forming substitutional metallofullerenes. Density functional theory calculation was performed to determine the structures of the model metallofullerenes $C_{53}Rh$ and $C_{54}M$ (M = Rh and Y). The calculated results are in general consistent with the experimental observations.

1. Introduction

The interactions of heteroatoms with fullerene cages are of particular interest in fullerene research because the chemical and physical properties of heterofullerenes are vastly different from those of pristine fullerenes. Three kinds of heterofullerenes are generally formed, that is, (1) the endohedral fullerenes with heteroatom(s) trapped inside the fullerene cage, (2) substitutional fullerenes with heteroatom(s) incorporated into the fullerene network by replacing one or more carbon atom(s), and (3) exohedral fullerenes with heteroatom(s) located outside the cage, in which the heteroatoms are usually attached to the fullerene cage via nonbonding interaction. Over the past decade, endohedral and substitutional fullerenes have been extensively studied because of their potential applications in many fields.[1−3] Both endohedral and substitutional fullerenes are usually produced by laser vaporization and arc discharge of graphite/metal composite rod at high temperature.[1,4,5] Alternative routes of producing endohedral metallofullerenes by Yang group,[6] and substitutional metallofullerenes by Branz et al.[7] and Poblet et al.[8] through interaction of heteroatoms with C_{60} cage were reported recently. Much progress has also been made on the theoretical studies of the geometric and electronic structures of heterofullerenes,[8,9,10−14] which provide insight to the elucidation of the formation processes of heterofullerenes.

Our recent laser ablation study of a series of externally doped metal fullerene clusters (metal fullerides) found that which type of metallofullerene will be formed by laser ablation depends strongly on the kinds of the metal atoms situated outside of the fullerene cage.[15] In this paper, we report on the contrasting behaviors of metal fullerides $C_{60}Rh_x$ and $C_{60}M_x$ (M = La, Y) under laser ablation. Theoretical calculations of the geometrical structures and electronic properties of the model metallofullerenes $C_{53}M$ and $C_{54}M$ were performed by the density functional theory to help in understanding the experimental results.

2. Experimental and Computational Methods

2.1. Sample Preparation. The metal fullerides $C_{60}M_x$ (M = Rh, La, Y, $x \approx 1$) were synthesized by the reactions of C_{60}^{3-} generated chemically in the THF solution phase with anhydrous metal trichlorides $RhCl_3$, $LaCl_3$, and YCl_3, respectively (molar ratio $C_{60}/M \approx 1$) under a dry argon atmosphere. The resulting solid powder was washed, centrifuged, and dried under vacuum. These compounds are characterized by electron probe microanalysis (EPMA), scanning electron microscopy (SEM), Fourier transform infrared spectroscopy (FTIR), thermal gravimetric analysis (TGA), and elemental analysis. The x values determined from elemental analysis show the nominal compositions of the metal fullerides. The structures of $C_{60}M_x$ and the interaction or bonding between M and C_{60} are not clear; they may be different for different metals. Very probably these samples are not homogeneous single-phase materials. These metal fullerides are air-stable and insoluble in common organic solvents. The powder sample was glued onto a stainless steel plate for laser ablation experiment.

To clarify the formation of endohedral metallofullerenes from the metal fullerides $C_{60}M_x$ (M = La, Y) under laser ablation, a composite sample that was shown to produce endohedral metallofullerene species under laser ablation was also studied

* To whom correspondence should be addressed. E-mail: lzhao@srcap.stc.sh.cn.
† Department of Physics.
‡ State Key Laboratory for Advanced Photonic Materials and Devices.
§ Department of Chemistry & Laser Chemistry Institute.

10.1021/jp027557g CCC: $25.00
Published on Web 04/18/2003

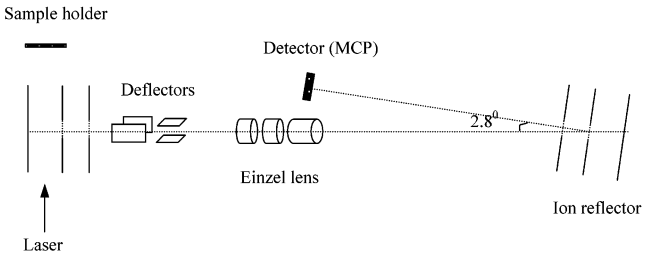

Figure 1. Schematic diagram of the reflectron time-of-flight mass spectrometer (RTOF).

under the same experimental conditions. The composite sample is a mixture of Y_2O_3 and ozonized C_{60} obtained by the reaction of C_{60} in toluene solution with O_3 gas generated from a discharge generator. The composite sample is pressed into pellet from a 1:1 (weight ratio) mixture of Y_2O_3 and ozonized product of C_{60}.

The purity of the C_{60} sample used in all synthesis reactions is better than 99.9% C_{60}. Laser ablation mass spectrometric characterization shows no mass peaks of other fullerenes. The C_{60} sample was obtained from Yin-Han Fullerene High-Tech. Co. Ltd., Wuhan University of China. $RhCl_3$ (analytical grade) was purchased from Acros Organics. Anhydrous lanthanide trichlorides, $LaCl_3$ and YCl_3, were prepared according to the literature procedure.[16]

2.2. Mass Spectrometric Measurements. The reflectron time-of-flight mass spectrometer (TOF-MS) used for laser ablation has been described in detail previously[17] and only a brief discussion will be given here. Figure 1 gives a schematic of the experimental setup in which the sample plate was placed in a position about 5 cm from the acceleration region of the spectrometer. A 308 nm XeCl excimer laser beam (~20 ns) was focused onto the sample with a 30 cm focal length lens in a direction perpendicular to the acceleration fields. The laser-ablated neutral and ionic species, together with electrons, were expanded into the acceleration region where the ions are accelerated. For the detection of negative ions, a pulsed voltage of −1200 V was applied on the double stage ion source. After double stage acceleration, the ions drifted along the axis of the field-free tube at ground potential. An Einzel lens was used to focus the ions into the reflector, which allows a second-order space focusing of the ions. In the reflection region, the ions were decelerated and reflected by a constant voltage of −1300 V applied on the reflector and then drifted at an angle of 2.8° from the incidence direction. The total field-free flight path was 1800 mm. The ions are detected by a triple-microchannel plate detector followed by a transient digitizer controlled with a computer. For the detection of positive ions, positive voltages were applied on the ion source and the reflector. All spectra reported in this paper were averaged over 30 laser shots. The mass resolution of the reflectron TOF is $M/\Delta M \approx 1000$.

2.3. Structural and Electronic Computation. Structure optimization was performed on model metallofullerenes $C_{53}M$ and $C_{54}M$. All calculations were performed by means of Gaussian 98 program package with the density functional theory using B3LYP for the exchange and the correlation corrections. The 3-21G basis set was used for both rhodium and yttrium systems. But for the yttrium system, the STO-3G basis set was also used for helping structure optimization and for comparison. The metallofullerene structures were optimized self-consistently starting from the metal-containing geometrical configurations derived from the all-carbon structures C_{54} and C_{55}, which were also optimized at the B3LYP/3-21G level without imposing any symmetry constraints on the structures. The convergence

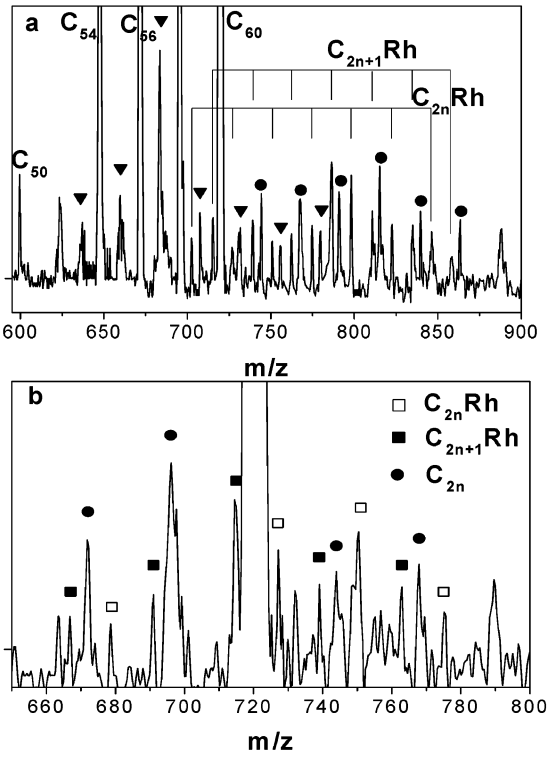

Figure 2. The laser ablation mass spectra of metal fulleride $C_{60}Rh_x$ (a) in the negative ion channel (● and ▼ denote the even- and odd-numbered carbon clusters) and (b) a portion of the positive ion mass spectrum in the mass range between 650 and 800 amu.

criterion is 10^{-5} au on the energy in general case and 10^{-4} au for cases hard to achieve convergence. The vertical ionization potentials and electron affinities of the metallofullerences were obtained by calculating the single-point energies of the cations and anions of the optimized neutral structures at the same level.

3. Results and Discussions

3.1. Formation of Metallofullerenes from $C_{60}Rh_x$ and $C_{60}M_x$ (M = La, Y) by Laser Ablation. Figure 2 shows the mass spectra recorded during 308 nm XeCl excimer laser ablation of $C_{60}Rh_x$ in the negative and positive ion modes. Two sequences $[C_{2n}Rh]^-$ and $[C_{2n+1}Rh]^-$ ($2n = 50-62$) with odd and even total number of atoms, respectively, are observed in the negative ion channel. These two rhodium-containing sequences display also in the positive ion mode but with narrower mass range. In our laser ablation experiments, only one high-energy laser was employed for fragmentation and ionization to form neutral and positive ionic species. For the formation of negative ions, electrons formed in the laser ablation process are attached to the neutral fullerene and metallofullerene species.

The negative ion mass spectrum provides much novel information not reported previously. Figure 2a reveals that four sequences of mass signals are formed in the negative ion channel: two of metallofullerenes, $C_{2n}Rh$ ($2n = 50-62$) and $C_{2n+1}Rh$ ($2n + 1 = 51-63$) and two of all-carbon clusters C_{2n} ($2n = 50-72$) and C_{2n+1} ($2n + 1 = 53-65$), both with one composed of even and one composed of odd numbers of carbon atoms. These results are quite different from the previous reports of Branz et al.[7] and Poblet et al.[8] In their laser ablation TOFMS study of metal fullerides $C_{60}M_x$ (M = Pt, Rh, Fe, Ir), only substitutional metallofullerenes with even numbers of total atoms were observed in the positive ion mass spectra. Although our sample and theirs are all exohedral, they are prepared by totally different methods and so have very different composition and

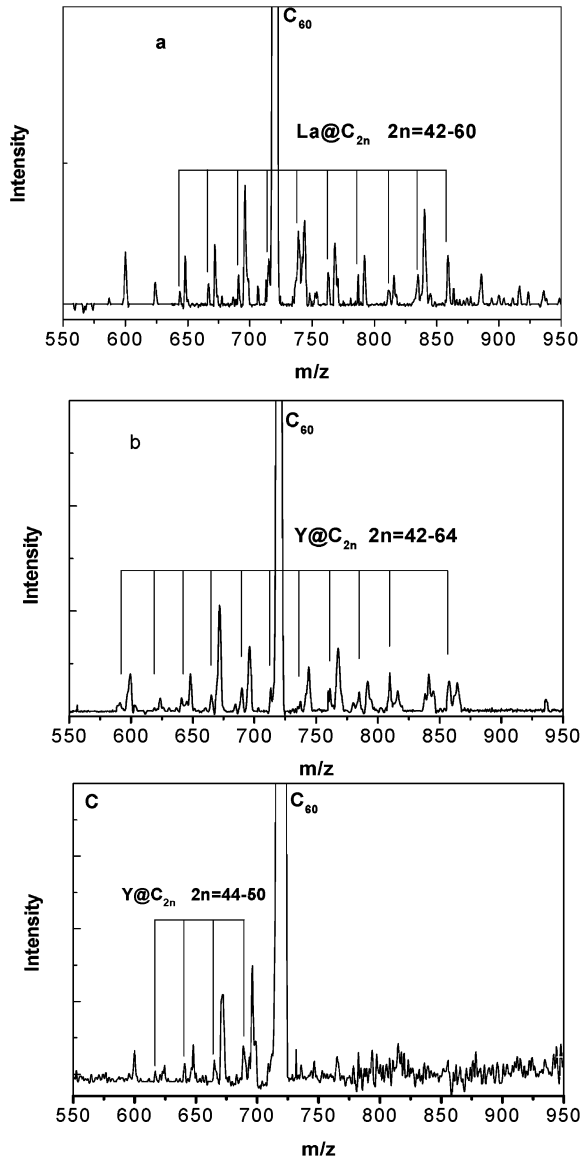

Figure 3. Typical positive ion TOF mass spectra of metal fullerides (a) $C_{60}La_x$, (b) $C_{60}Y_x$, and (c) the composite material $(C_{60} + O_3)/Y_2O_3$ obtained with a laser influence of about 700 mJ/cm^2.

properties. The simultaneous formation of both C_{2n}Rh and C_{2n+1}Rh sequences in both ion modes in our case is particularly interesting and deserves further investigation. The sequence C_{2n+1}Rh recorded here is similar to those reported previously; the substitutional structure characteristic is generally accepted. The most interesting result is the appearance of the sequence C_{2n}Rh with odd numbers of total atoms. The absence of endohedral evidence for C_{2n}Rh sequence (see below for the La and Y case) asks us to consider other structure possibilities. The simultaneous appearance of metallofullerene C_{2n}Rh ($2n$ = 50−62) and all-carbon C_{2n+1} ($2n$ = 52−64) sequences with odd numbers of total atoms in the nearly same $2n$ range attracts our attention. On the basis of the parallelism between these two sequences, we suggest that C_{2n}Rh will take the substitutional structure with the Rh atom replacing the 2-fold coordinated carbon in the C_{2n+1} structure. We will discuss this problem in detail in section 3.2.

Figure 3 shows the positive ion mass spectra taken from the laser ablation of metal fullerides $C_{60}La_x$ and $C_{60}Y_x$ and also the composite material $(C_{60}+O_3)/Y_2O_3$ under a fluence of about 700 mJ/cm^2. A sequence of metallofullerenes, C_{2n}La ($2n$ = 42−60) or C_{2n}Y ($2n$ = 42−64), is formed. The "shrink wrap" behavior[18] in the fragmentation of the metallofullerene sequence gives evidence of the endohedral nature of the metallofullerenes. Previous theoretical calculations predict that the encaged La in C_{60} possesses a formal charge of +3,[19] and La^{3+} has an ionic radius of 1.06 Å,[20] so it can form metallofullerenes of small sizes. Yang et al.[6] demonstrated the endohedral nature of the metallofullerenes formed in the laser ablation of the C_{60}/La_2O_3 composite. The formation of endohedral metallofullerenes in our case is similar to theirs in the encapsulation mechanism, which has been discussed in our previous report.[21]

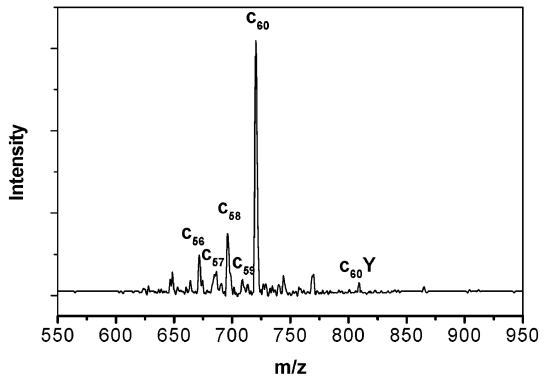

Figure 4. Typical negative ion TOF mass spectrum of metal fulleride $C_{60}Y_x$ with a laser fluence of about 650 mJ/cm^2.

In the negative ion channel, no metallofullerenes of La or Y were observed except $C_{60}La^-$ and $C_{60}Y^-$, which might come from the precursors after evaporating part of the metal atoms and subsequently seizing an electron. The negative ion mass spectrum of $C_{60}Y_x$ in Figure 4 illustrates the sharp contrast with the positive ion mass spectrum. The absence of anionic metallofullerenes $C_{2n}Y^-$ ($2n \neq 60$) might be another indication of the endohedral nature of these metallofullerenes. It seems that the exohedral metallofullerenes and substitutional metallofullerenes appear in both ionic modes as shown in Figure 2, but the endohedral ones appear only in the positive ion channel.

The reason is not clear. The Hettich group[22] reported a similar result in their investigation of the fragmentation of endohedral metallofullerene La@C_{60}. They observed endofullerenes in the FTICR negative ion mass spectrum but were unable to observe the negative endofullerene ions in the LD-TOFMS experiments. They attributed the contrast to the long electron−molecule interaction time in the FTICR cell. The negative ions of the ablation products are formed through electron attachment. Both the magnitude of the electron affinities and the kinetics of electron attachment influence this process. The electron affinities of metallofullerenes are generally larger than those of empty fullerenes. The presence of empty fullerene sequence C_{2n}^- but not the metallofullerene sequence $C_{2n}Y^-$($2n \neq 60$) is somewhat surprising. The kinetics of the formation of endometallofullerenes might play a key role. It is very probable that the endometallofullerene is formed through a quite slow process so that the neutral species M@C_{2n} formed in our laser ablation mass spectrometer has no chance to catch electron to form anions.[23] In Hettich's FTICR cell, the electron−molecule interaction time is >1 ms,[22] but in our case the plasma generated from laser ablation takes only ∼0.1 ms to reach the acceleration region, which limits the interaction of electron with neutral endofullerene to form anions.

From the mass spectra depicted in the preceding figures, sharp contrast can be found in the behavior of metallofullerene formation from Rh fulleride and Y (or La) fulleride. The main features are as follows: (1) Rhodium metallofullerenes are

formed both in the negative and in the positive ion channels, the negative ion mass spectrum being much better than the positive one. In contrast, the yttrium (or lanthanum) metallofullerenes appear only in the positive ion mass spectrum. (2) Two sequences of rhodium metallofullerenes with even and odd numbers of carbon atoms, respectively, $C_{2n}Rh$ and $C_{2n+1}Rh$, are formed, whereas for yttrium (or lanthanum), metallofullerene sequences with only even number of carbon atoms are formed. (3) In the mass spectrum of yttrium (or lanthanum) metallofullerene, evidence of forming endohedral structures is observed, whereas no such evidence appears in the rhodium case. Our observation of the formation of endohedral metallofullerenes of lanthanum and yttrium metals but not for rhodium metal is consistent with all of the previous reports.[23] Extensive work on endohedral metallofullerenes of La, Y, and Sc has been reported, but no substitutional metallofullerenes of La and Y have been observed. The case of rhodium is just the reverse; no formation of endohedral rhodium metallofullerene has ever been reported, and only substitutional metallofullerenes $C_{2n+1}Rh$ with even total number of atoms have been recorded.

3.2. Structural Properties of Metallofullerenes. *3.2.1. Structural Modeling of Metallofullerenes.* The structure investigation of metallofullerenes is a challenging task, both experimentally and theoretically. The development in the experimental technique of cluster structure determination and in the quantum chemical calculation of quite big molecular systems owing to the rapid progress in computer technique has produced breakthroughs in such investigation in recent years. Jarrold et al. had made significant contribution to the structural investigation of metallofullerenes. Their experiments using the gas-phase ion mobility technique provide conclusive evidence that $C_{2n+1}M$ heterofullerenes with an even number of total atoms in the high carbon region are closed cage structures with M networked on the cage.[9] In the theoretical aspect, early ab initio calculation by Jarrold and recent calculations on $C_{59}M$ (M = Si, Fe, Co, Ni, Rh) by other research groups all confirmed the experimental conclusion of networked cage structures.[8,10−14] On the basis of these experimental, as well as theoretical, results, we believe that the $C_{2n+1}Rh$ observed in our experiments also takes such substitutional networked cage structures with the rhodium atom replacing one of the carbon atoms in usual fullerene structures. For $C_{2n+1}Rh$, we calculated structures with various possible substitution sites and optimized the parameters. No calculation on $C_{2n+1}Y$ was made because no such substitutional metallofullerenes have been observed in our experiment. As to metallofullerenes with an odd number of total atoms $C_{2n}M$, that is, with an even number of carbon atoms together with one metal atom, the structure problem is more complicated and depends significantly on the properties of the metal atom involved, as shown in our experimental mass spectra. The La- and Y-containing metallofullerenes show the evidence of forming endohedral structures $M@C_{2n}$, but the Rh-containing ones show no such evidence. Metallofullerenes composed of an even number of carbon atoms but displaying no endohedral evidence have not been noticed in previous experiments, and no discussion on their structures has been reported. We will discuss the possible structures of $C_{2n}Rh$ and $C_{2n}Y$ on the basis of density functional calculations. No metallofullerenes with more than one metal atom have been detected in our experiments, so no calculation on such metallofullerene was made in this work.

Our experimental results show that the ranges of metallofullerenes formed in the laser ablation mass spectra are as follows: $C_{2n}Rh$ ($2n = 50-62$) and $C_{2n+1}Rh$ ($2n + 1 = 51-63$) in the negative ion MS; $C_{2n}La$ ($2n = 42-60$) and $C_{2n}Y$ ($2n = 42-64$) in the positive ion MS. So we take $C_{53}M$ and $C_{54}M$ as model molecules for our calculation. We construct the structures of $C_{53}M$ and $C_{54}M$ from the corresponding all-carbon structures C_{54} and C_{55}, respectively. The structures of the all-carbon clusters C_{54} and C_{55} were first optimized with a genetic algorithm based on the Brenner potential and then reoptimized at the B3LYP/3-21G level with Gaussian 98 program package. No imaginary frequencies are found for these two molecules optimized at the B3LYP/3-21G level, indicating that they are energy minima on the potential energy surfaces. The lowest energy structures of C_{54} and C_{55} are shown in Figure 5 and the corresponding energies in Table 1. C_{54} has the usual fullerene structure; Figure 5a shows the symmetry of the lowest energy structure. Figure 5b is the optimized structure of C_{55}. It takes the cagelike form as its lowest energy structure, but close inspection found that it is not the true closed-cage fullerene but is a quasi-cage containing a 2-fold coordinated carbon atom appending on the boundary of two pentagons. This C_{55} structure is a typical representative of the odd-numbered high carbon clusters, as given by our genetic calculation on $C_{51}-C_{59}$ (not shown here), in which the 2-fold carbon atom is appended on the pentagon/pentagon, pentagon/hexagon, or hexagon/hexagon boundary for different carbon clusters. We may call them pseudo-fullerenes. We know that for fullerenes there are many structural isomers some of which have similar energies. For odd-numbered all-carbon clusters, C_{2n+1}, we also found structural isomers slightly higher in energy than the minimum energy structure in Figure 5b. For example, in our calculation of C_{55} with genetic algorithm, the isomer next to the lowest energy minimum has an energy of −2083.6546 hartree after Gaussian optimization, higher in energy than the minimum structure by

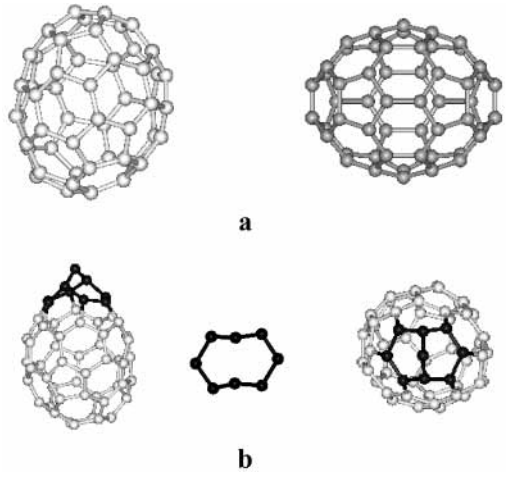

Figure 5. Optimized structure of C_{54} and the odd-numbered carbon cluster C_{55}: (a) two views of the lowest energy isomer of C_{54} showing the symmetry; (b) two views of the lowest energy isomer of C_{55} and the window formed by removing the 2-fold bonded appending carbon atom.

TABLE 1: Energies of the Optimized Structures of C_{54}, C_{55}, $C_{53}Rh$, $C_{54}Rh$, and $Rh@C_{54}$ Calculated at the B3LYP/3-21G Level

structures	species	energies (hartree)[a]
Figure 4a	C_{54}	−2045.9934
Figure 4b	C_{55}	−2083.6703
Figure 5a	$C_{53}Rh$ (666)	−6674.6139
Figure 5b	$C_{53}Rh$ (665)	−6674.6392
Figure 5c	$C_{53}Rh$ (655)	−6674.6755
Figure 5d	$C_{54}Rh$ (2-fold net)	−6712.4436
Figure 5e	$Rh@C_{54}$	−6712.5277

[a] The zero-point energy correction is not included.

only 0.4 eV. Its structure is similar to that shown in Figure 5b but with the 2-fold coordinated carbon atom appending on the boundary of two hexagons instead of two pentagons.

For the construction of $C_{53}Rh$, the Rh atom replaces one of the carbon atoms in C_{54}. Unlike C_{60}, in which all of the carbon sites are equivalent, in the C_{54} structure there are three kinds of carbon sites, the 666, 665, and 655 sites where the numbers 6 and 5 represent the hexagons and the pentagons forming the carbon site as shown in the figure. For the construction of C_{53}-Rh, the Rh atom may replace a carbon atom at one of these three different sites forming the structural isomers. For $C_{54}M$, the most interesting structure is the endohedral metallofullerene with the metal atom inside the C_{54} carbon cage. La(or Y)@C_{54} is really the case. But for $C_{54}Rh$, we have to consider the other possibility because the formation of Rh endohedral metallofullerene neither was observed in our experiments nor has ever been reported previously. As mentioned in previous section, a substitutional structure is suggested for $C_{54}Rh$. The 2-fold coordinated appending carbon atom in C_{55} provides an active site for substitution, because the breaking and formation of only two bonds holding this atom to the cage are involved in the substitution. On the basis of this consideration, we think that $C_{54}Rh$ may take quasi-cage structure with a Rh atom substituting the appending C atom. For comparison, we calculate both the endohedral structure and the quasi-cage substitutional structure for Rh and Y metallofullerenes $C_{54}M$. The formation of the metallofullerenes calculated in this paper is illustrated as follows:

$$C_{54} \rightarrow \text{Rh substitution} \rightarrow C_{53}Rh \quad \text{(Rh at 666 site)}$$
$$\rightarrow \text{Rh substitution} \rightarrow C_{53}Rh \quad \text{(Rh at 665 site)}$$
$$\rightarrow \text{Rh substitution} \rightarrow C_{53}Rh \text{ (Rh at 655 site)}$$

$$C_{54} \rightarrow \text{Rh insertion} \rightarrow Rh@C_{54}$$
$$\rightarrow \text{Y insertion} \rightarrow Y@C_{54}$$

$$C_{55} \rightarrow \text{Rh substitution} \rightarrow C_{54}Rh \text{ (Rh at 2-fold site)}$$
$$\rightarrow \text{Y substitution} \rightarrow C_{54}Y \text{ (Y at 2-fold site)}$$

No calculations on lanthanum metallofullerenes have been made, but we think that their structures might be similar to those of yttrium ones.

3.2.2. Geometric Structures of $C_{53}Rh$ and $C_{54}M$ (M = Rh, Y). The geometric structures of all of the rhodium metallofullerenes are optimized at the B3LYP/3-21G level. The energies of the optimized structures are presented in Table 1, and the corresponding structures are depicted in Figure 6. We tried to do the optimization of the yttrium metallofullerenes at the same level. There is no problem for the endohedral metallofullerene $Y@C_{54}$, but optimization convergence could not be achieved for the networked metallofullerene $C_{54}Y$ in which Y atom is 2-fold connected to the carbon cage. For this reason, the geometric structure of $C_{54}Y$ was first optimized at the B3LYP/STO-3G level and then reoptimized at the B3LYP/3-21G level. In the calculation of yttrium metallofullerenes, level shift method and quadratically convergent SCF procedure were used to enforce convergence. Even in so doing, convergence could not be achieved in some cases. The calculated results were presented in Table 2, and the corresponding structures were depicted in Figure 7. The structural parameters of the optimized metallofullerene isomers are presented in Table 3.

The binding energy of C_{55} is 8.46 eV/atom, which is 0.10 eV/atom less than that of C_{54}, indicating that the former is less

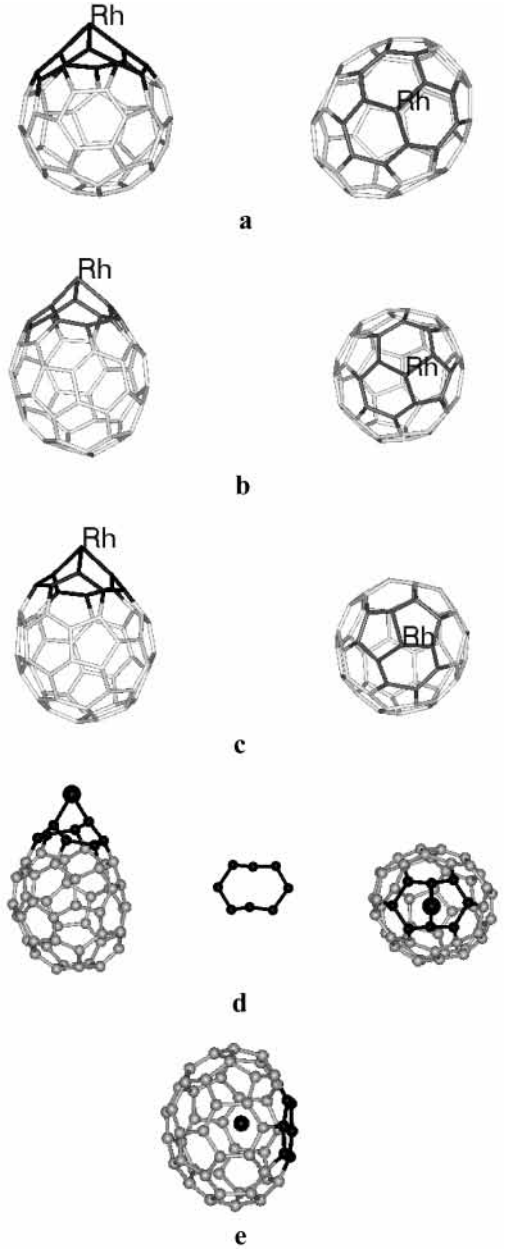

Figure 6. The optimized structures of the rhodium metallofullerenes: (a) two views of the lowest energy isomer of $C_{53}Rh$ (666); (b) two views of the lowest energy isomer of $C_{53}Rh$ (665); (c) two views of the lowest energy isomer of $C_{53}Rh$ (655); (d) two views of the lowest energy isomer of $C_{54}Rh$ (networked) and the window formed by removing the 2-fold bonded appending rhodium atom; (e) the lowest energy isomer of $Rh@C_{54}$ (the solid circles denote the metal atom (bigger circle) and the carbon atoms of the nearest hexagon).

stable than the latter. All of the isomers of $C_{53}Rh$ still keep the cage structure but are distorted because of the substitution of a carbon atom by the bigger Rh atom. From the energies shown in Table 1 and the bond lengths shown in Table 3, we know that the structural isomers of $C_{53}Rh$ have very similar structural parameters and binding energies. The bond lengths between rhodium and its neighboring carbon atoms are similar for the three isomers, ranging from 1.94 to 1.98 Å, and the C−C bond lengths are also similar, ranging from 1.38 to 1.50 Å. The binding energies of the isomers differ by less than 0.03 eV/atom, ranging from 8.45 to 8.48 eV/atom, which are 0.08−0.11 eV/atom smaller than that of C_{54}. The electron charge transfers from Rh atom to the nearest carbon neighbors are also similar for the different isomers. The atomic charge on Rh atom

TABLE 2: Energies of the Optimized Structures of $C_{54}Y$ and $Y@C_{54}$ Calculated at the B3LYP/3-21G and B3LYP/STO-3G Levels

structures	species	energies (hartree)[a]	model level
Figure 6a	$C_{54}Y$ (2-fold net)	−5331.0684	B3LYP/STO-3G
		−5363.8179	B3LYP/3-21G
		−5363.7847	B3LYP/3-21G// B3LYP/STO-3G
Figure 6b	$Y@C_{54}$	−5331.2790	B3LYP/STO-3G
		−5364.0381	B3LYP/3-21G
		−5364.0101	B3LYP/3-21G// B3LYP/STO-3G

[a] The zero-point energy correction is not included.

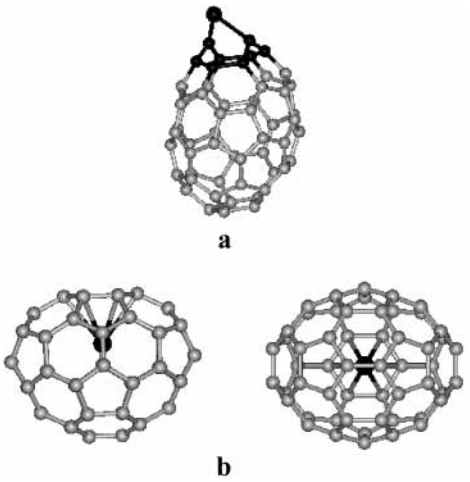

Figure 7. The optimized structures of the yttrium metallofullerenes: (a) the lowest energy isomer of $C_{54}Y$(networked); (b) two views of the lowest energy isomer of $Y@C_{54}$ showing the symmetry. The solid circle denotes the metal atom.

TABLE 3: The Bond Lengths (or Distances) and Binding Energies for C_{54}, C_{55}, $C_{53}Rh$, $C_{54}M$, and $M@C_{54}$ (M = Rh, Y) Structures Optimized at the B3LYP/3-21G Level

species	M−C (Å)	C−C (Å)	binding energy (eV/atom)
C_{54}		1.37−1.50	8.56
C_{55}		1.37−1.52	8.46
$C_{53}Rh$ (666)	1.94, 1.95, 1.95	1.38−1.50	8.45
$C_{53}Rh$ (665)	1.94, 1.95, 1.98	1.38−1.49	8.47
$C_{53}Rh$ (655)	1.94, 1.97, 1.98	1.38−1.50	8.48
$C_{54}Rh$ (2-fold net)	1.94, 1.95	1.37−1.53	8.43
$Rh@C_{54}$	2.55−2.84	1.39−1.48	8.47
$C_{54}Y$ (2-fold net)	2.15, 2.15	1.37−1.51	8.39
$Y@C_{54}$	2.45−2.55	1.39−1.48	8.51

is positive, ranging from 0.9 to 1.0. We have presented only the structural isomers of $C_{53}Rh$ derived from the lowest energy C_{54}. Isomers of $C_{53}Rh$ derived from other C_{54} isomers with energies not too much higher than those presented here may also appear in the laser ablation products. Therefore, it is reasonable to believe that $C_{53}Rh$ and other $C_{2n+1}Rh$ metallofullerenes formed in laser ablation consist of many isomers with similar energies.

In the networked metallofullerene $C_{54}M$, the metal atom Rh or Y is 2-fold coordinated. No imaginary frequencies are found for the $C_{54}Rh$ molecule calculated at the B3LYP/3-21G level, indicating that it is an energy minimum on the potential energy surface. In $C_{54}Rh$, the Rh−C bond lengths are 1.94−1.95 Å, and the C−C bond lengths range from 1.37 to 1.53 Å. The corresponding values in $C_{54}Y$ optimized at the B3LYP/3-21G level are 2.15 Å and 1.37−1.51 Å. The binding energy of C_{54}-Rh is a little smaller than that of $C_{53}Rh$ and C_{55}. The structures of the endohedral metallofullerenes $Rh@C_{54}$ and $Y@C_{54}$ are shown in Figure 6e and Figure 7b. From the distances of the metal atom to the surrounding carbon atoms, we found that the metal atom is situated closer to a hexagon with higher electron density. The distances from the metal atom to the six carbon atoms of this hexagon are from 2.5 to 2.8 Å for $Rh@C_{54}$ and from 2.45 to 2.55 Å for $Y@C_{54}$. The atomic charge on Rh atom is +0.62 for networked $C_{54}Rh$ and +1.39 for endohedral $Rh@C_{54}$. The corresponding values for yttrium compounds are +1.27 and +2.14. From the position and the charge of the trapped ion in the cage, we can see that there exists stronger interaction between the yttrium ion and the surrounding carbon cage, which greatly stabilizes the endohedral yttrium metallofullerene. The endohedral $Rh@C_{54}$ has binding energy a little (0.04 eV) higher than the corresponding networked $C_{54}Rh$. It is interesting to find that the binding energy of the endohedral $Y@C_{54}$ is much (0.12 eV) higher than that of $C_{54}Y$. It seems that from a thermodynamic point of view metallofullerenes $C_{54}M$ would like to form the more stable endohedral isomers; the tendency is much stronger in the yttrium case. In fact, this is not the only facter. The properties of the metal play a key role in determining which type of isomer structure will really be formed. Here we have the typical case that Y atom is prone to enter the fullerene cage, whereas the networked structures are more favorable to Rh metallofullerenes. The stability of the endohedral isomers compared to those of the networked isomers is higher for Y than for Rh; this is in accord with the experimental results. Similar to the case of $C_{2n+1}Rh$, isomers of metallofullerenes $M@C_{2n}$ and $C_{2n}M$ (networked) with similar energies may be present, for example, $Y@C_{54}$ isomers other than that shown in Figure 7b may be derived from C_{54} isomers other than the lowest energy minimum. Moreover, as cited by Shinohara that Dennis and Takata pointed out,[24] the presence of the metal may cause the stability order of the metallofullerene isomers to become different from that of the corresponding empty fullerenes. That is to say, the $Y@C_{54}$ shown here may not be the lowest energy isomer. We will not discuss the case of endohedral metallofullerenes further, because it has been discussed in previous papers.[24] For the networked metallofullerene, we made calculation on the $C_{54}Rh$(net) isomer derived from the C_{55} isomer next in energy to the lowest energy minimum. It was found that after Gaussian optimization the energy of this isomer is higher than the value of the $C_{54}Rh$(net) isomer shown in Table 1 by only 0.3 eV. It is very probable that the $C_{54}Rh$(net) shown in Table 1 is the lowest energy isomer of the networked metallofullerene, but there exist many structural isomers of networked metallofullerenes $C_{2n}Rh$ with similar energies, which will form simultaneously in our laser ablation experiments.

Our calculation illustrating the possibility of $C_{2n}Rh$ to take the networked structure with the Rh atom situated in the 2-fold coordinated position is only preliminary. This structure supposition has to be verified by experimental and further theoretical investigations.

3.3. Discussion on the "Window" Mechanism of Endofullerene Formation. The formation of endohedral metallofullerene has been investigated experimentally and theoretically in recent years. A window mechanism has been proposed to account for the insertion of guest atom into the fullerene cage, in which one or more bonds are broken to open a temporary "window" in the cage allowing easy incorporation of the guest atom. But detailed calculation about the helium incorporation into fullerene cage by Thiel's group revealed that the activation

barriers for the insertion of He through the one-bond windows and two-bond windows are similar to that through a hexagon, so are still very high.[25] For the insertion of metal atom like Rh or Y, the barrier will be even higher. Here we would like to have an estimation of the barrier of the passage of metal atom through the window formed on the odd-numbered carbon cage, C_{55}, through the cleavage of the 2-fold coordinated carbon atom or the window formed on the networked $C_{54}Rh$ through the cleavage of the 2-fold coordinated Rh atom. Take the latter case for discussion. The atomic sizes of Rh and Y are 1.3 and 1.6 Å, respectively. From our calculation of the supposed endohedral structures $M@C_{54}$, the charges on the inside atom are +1.39 and +2.14 for Rh and Y, respectively. The sizes of Rh^{+2} and Y^{+3} are 0.86 and 0.93 Å, respectively.[20] After correction for the charges on the atoms, the sizes of the Rh and Y ions in C_{54} can be estimated to be approximately 0.9 and 1.0 Å, respectively. These sizes are comparable to the atomic size of He. According to the "window" mechanism for the transition of external metal atom into the interior of the cage, it must pass through the window formed by the neighboring eight carbon atoms after the cleavage of the metal atom. As shown in Figure 6d, the small window formed from networked $C_{54}R$ possesses a narrow long shape with an entrance width of only 2.3 Å, which is even narrower than the one-bond window formed on C_{60} in Thiel's case.[25] Because of this unfavorable shape of the window and the big size of the metal atom treated here, the metal insertion through the window must overcome a very high barrier, if the window remains rigid. If metal ions are formed in the plasma, the situation might be slightly better. Of course the window can deform to accommodate the metal atom or ion insertion, but the barrier is still much too high for the incoming atom or ion to squeeze through. The estimated value might reach tens of electronvolts. The difference in stability of the networked $C_{54}Rh$ and the endohedral $Rh@C_{54}$ is only 2.3 eV. It is quite reasonable to suppose that $C_{54}Rh$ and other $C_{2n}Rh$ will take the networked structure rather than have the metal atom to squeeze into the cage to form endohedral ones. As to the Y case, the endohedral $Y@C_{54}$ structure is 5.9 eV more stable than the networked structure, and Y is one of the metal elements that are preferentially to be trapped inside the fullerene cage. Therefore it is not surprising that yttrium metallofullerenes only take the endohedral structure $Y@C_{2n}$. But even in this case, the endofullerene formation cannot be explained by the simple window mechanism supposed above. The bigger size of the yttriun atom or ion makes the insertion process even more difficult. Therefore the formation mechanism of endometallofullere is still a problem to be further investigated.

3.4. Vertical Ionization Potentials and Electron Affinities of $C_{54}M$ and $M@C_{54}$ with M = Rh and Y. We have pointed out the contrasting behaviors of rhodium and yttrium in forming metallofullerenes through laser irradiation of metal fullerides; one important point is the difference in the two ion modes. Yttrium metallofullerenes, most probably in the form of endohedral structures, are formed only in the positive ion channel, whereas rhodium metallofullerenes, most probably in the form of substitutional networked structures, are formed more effectively in the negative ion channel, both in intensities and in mass range. To get some insight to explain these phenomena, we have calculated the vertical ionization potentials (IPs) and the vertical electron affinities (EAs) of C_{54}, C_{55}, $C_{54}Rh$ (networked), and $Rh@C_{54}$. For the all-carbon clusters and the rhodium metallofullerenes, the single-point energies of the neutral molecules, the corresponding cations, and anions are calculated at the B3LYP/3-21G level on structures of the neutral molecules optimized at the same level. The calculated values of C_{54}, C_{55}, $C_{54}Rh$ (networked), and $Rh@C_{54}$ are presented in Table 4.

TABLE 4: The Vertical Ionization Potentials and Electron Affinities for C_{54}, C_{55}, $C_{54}Rh$ (networked), and $Rh@C_{54}$ at the B3LYP/3-21G Level

species	IP (eV)	EA (eV)
C_{54}	7.18	3.22
C_{55}	7.25	2.80
$C_{54}Rh$ (networked)	7.14	2.37
$Rh@C_{54}$	8.16	2.16

TABLE 5: The Single-Point Cationic and Anionic Energies of $Y@C_{54}$ and $C_{54}Y$ (networked) Calculated at the B3LYP/STO-3G and B3LYP/3-21G Levels on Geometrical Structures Optimized at the Same Level

species	energies (hartree) at the B3LYP/STO-3G level	energies (hartree) at the B3LYP/3-21G level
$Y@C_{54}$	−5331.2790	−5364.0381
$[Y@C_{54}]^+$	−5331.1380	−5363.7233
$[Y@C_{54}]^-$	−5331.2293	−5363.9438
$C_{54}Y$ (networked)	−5331.0684	−5363.8179
$[C_{54}Y]^+$	−5330.9217	−5363.5859
$[C_{54}Y]^-$	−5331.0625	−5363.8932

The experimental IP and EA of C_{60} are 7.6 and 2.7 eV, respectively. In general, the IP of fullerene lowers and the EA increases with the size of fullerene, so our calculated values for C_{54} are too low in IP and too high in EA. For metallofullerene with the metal atom situated either inside the cage or incorporated in the network, the IP is usually lower and the EA is usually higher than the empty fullerene of the same size. Taking the size and the metal effects into account, the calculated IP of $Rh@C_{54}$ in the table is too high and the EA is too low compared to the expected values. Therefore the absolute values in Table 4 are not acceptable. Nevertheless, the comparison between the calculated values of the networked $C_{54}Rh$ and the endohedral $Rh@C_{54}$ indicates the same trend as that shown by the experimental mass spectra. Our calculation indicates that the networked $C_{54}Rh$ has much lower ionization potential and higher electron affinity than $Rh@C_{54}$. This is in reasonable agreement with the experiments, which show that rhodium metallofullerenes are prone to form networked structures rather than endohedral structures both in the negative and in the positive ion modes.

The single-point energies of the cations and anions of $C_{54}Y$ and $Y@C_{54}$ were calculated at the B3LYP/STO-3G and B3LYP/3-21G levels, respectively, and the results are shown in Table 5. As stated above, level shift method and quadratically convergent SCF procedure were used to enforce convergence, and quite low convergence had to be used in our calculations of yttrium metallofullerenes.

From the energy values shown in the table, the ionization potential of $Y@C_{54}$ is calculated to be 8.4 eV at the B3LYP/3-21G level. The reported calculation value of $Y@C_{82}$ is 6.22 eV.[26] After correction for the size of the cage, our calculation value at the B3LYP/3-21G level is still too high for endohedral metallofullerene of this size. The B3LYP/STO-3G value is much too low (∼3.8 eV), showing that the STO-3G basis set is too small for the Y-containing metallofullerenes. It is worth noting that our calculation gave a negative value to the electron affinity of $Y@C_{54}$ at the B3LYP/3-21G level. Maybe this is an indication that the endohedral $Y@C_{2n}$ are prone to form positive ions but have little tendency to form negative ions so that they only appear in the positive ion mass spectrum recorded in our experiments. However, there may be other factors that account

for this phenomenon, as discussed in the experimental part of this paper. As to networked $C_{54}Y$, the ionization potential and electron affinity calculated at the B3LYP/3-21 level are 6.21 and 2.05 eV, respectively. It seems that networked $C_{54}Y$ would appear in the positive and negative ion mass spectra, but no experimental support could be found. In general, our calculation on Y metallofullerenes is not satisfactory.

Our theoretical investigation on the electronic properties of metallofullerenes is preliminary; higher level calculation is necessary, especially for the yttrium metallofullerenes.

4. Conclusions

Laser ablation−TOF mass spectrometry study of externally doped metal fullerides $C_{60}Rh_x$ and $C_{60}M_x$ (M = La, Y) reveals the contrasting behaviors of Rh and Y (La) in metallofullerene formation. DFT study of the model metallofullerenes indicates that different substitutional isomers of $C_{2n+1}Rh$ with similar energies will be formed under laser ablation. The endohedral metallofullerenes $Rh@C_{54}$ and $Y@C_{54}$ are calculated to be more stable than the 2-fold networked structures $C_{54}Rh$ and $C_{54}Y$ by 2.3 and 5.9 eV, respectively. The vertical ionization potentials (IPs) and electron affinities (EAs) of the model molecules $C_{54}M$ (networked) and $M@C_{54}$ (M = Rh,Y) calculated at the B3LYP/3-21G level show that the networked molecule $C_{2n}Rh$ has lower IP and higher EA than the endohedral molecule $Rh@C_{2n}$, favoring the formation of the former both in the positive and negative ion modes. The EA of $Y@C_{54}$ is calculated to be a negative value at the B3LYP/3-21G level; this is in accord with the absence of $Y@C_{2n}$ in the negative ion mass spectrum. In conclusion, rhodium metallofullerenes usually take the substitutional structures $C_{2n+1}Rh$ and $C_{2n}Rh$ and appear in both ionic modes, whereas yttrium/lanthanum metallofullerenes are prone to take the endohedral structures and appear usually in the positive ion modes. Theoretical calculation can interpret the main features of rhodium metallofullerenes but leaves many problems open in the yttrium case, including the formation mechanism of the endohedral metallofullerenes.

Acknowledgment. The support of this work by The National Natural Science Foundation of China, Project Nos. 29890216 and 20271013, and the National High Performance Computing Center, Shanghai, China, is greatly acknowledged. We are grateful to Dr. Chen Zhongfang from the Max Planck Inst Kohlenforsch, D-45470 Mulheim, Germany, for the helpful discussions and assistance in theoretical calculations. We are also grateful to the Computational Chemistry Laboratory, Department of Chemistry, Fudan University, for the assistance in performing the Gaussian calculations.

References and Notes

(1) Bethune, D. S.; Johnson, R. D.; Salem, J. R.; De Vries, M. S.; Yannoni, C. S. *Nature* **1993**, *366*, 123.
(2) Shinohara, H. *Adv. Met. Semicond. Clusters* **1998**, *4*, 205.
(3) Shinohara, H.; Tanaka, M.; Sakata, M.; Hashizume, T.; Sakurai, T. *Mater. Sci. Forum* **1996**, *232*, 207.
(4) Guo, T.; Jin, C.; Smalley, R. E. *J. Phys. Chem.* **1991**, *95*, 4948.
(5) Andreoni, W.; Gygi, F.; Parinello, M. *Chem. Phys. Lett.* **1992**, *190*, 159.
(6) Yang, S. H.; Huang, R. B.; Lu, W. Y. *Surf. Rev. Lett.* **1996**, *3*, 803.
(7) Branz, W.; Billas, I. M. L.; Malinowski, N.; Tast, F.; Heinebrodt, M.; Martin, T. P. *J. Chem. Phys.* **1998**, *109*, 3425.
(8) Poblet, J. M.; Munoz, J.; Winkler, K.; Cancilla, M.; Hayashi, A.; Lebrilla, C. B.; Balch, A. L. *Chem. Commun.* **1999**, 493.
(9) Clemmer, D. E.; Hunter, J. M.; Shelimov, K. B.; Jarrold, M. F. *Nature* **1994**, *372*, 248.
(10) Ding, C. G.; Yang, J. L.; Cui, X. Y. *J. Chem. Phys.* **1999**, *111*, 8481.
(11) Shelimov, K. B.; Clemmer, D. E.; Jarrold, M. F. *J. Phys. Chem.* **1994**, *98* (49), 12819.
(12) Chen, Z. F.; Ma, K. Q.; Shang, Z. F.; Pan, Y. M.; Zhao, X. Z.; Tang, A. Q. *Acta Chim. Sin.* **1999**, *57*, 712.
(13) Billas, I. M. L.; Massobrio, C.; Boero, M.; Parrinello, M.; Branz, W.; Tast, F.; Malinowski, N.; Heinebrodt, M.; Martin, T. P. *J. Chem. Phys.* **1999**, *111*, 6787.
(14) Billas, I. M. L.; Massobrio, C.; Boero, M.; Parrinello, M.; Branz, W.; Tast, F.; Malinowski, N.; Heinebrodt, M.; Martin, T. P. *Comput. Mater. Sci.* **2000**, *17*, 191.
(15) Kong, Q. Y.; Shen, Y. F.; Zhao, L.; Zhuang, J.; Qian, S. X.; Li, Y. F.; Lin, Y. H.; Cai, R. F. *J. Chem. Phys.* **2002**, *116*, 128.
(16) Tayler, M. D.; Carter, C. P. *J. Inorg. Nucl. Chem.* **1962**, *24*, 387.
(17) Kong, Q. Y.; Zhuang, J.; Zhao, L.; Qian, S. X.; Li, Y. F.; Cai, R. F.; Hou, H. Q. *Int. J. Mass Spectrom.* **2001**, *209*, 69.
(18) Weiss, F. D.; O'Brien, S. C.; Elkind, J. L.; Curl, R. F.; Smalley, R. E. *J. Am. Chem. Soc.* **1988**, *110*, 4464.
(19) Laasonen, K.; Andreoni, W.; Parinello, M. *Science* **1992**, *258*, 1916.
(20) *Lange's Handbook of Chemistry*, 13th ed; Dean, J. A., Ed.; McGrawHill: New York, 1985.
(21) Kong, Q. Y.; Shen, Y. F.; Xu, J.; Zhao, L.; Zhuang, J.; Qian, S. X.; Li, Y. F.; Li, X.; Lin, Y. H.; Cai, R. F. *Chem. Phys. Lett.* **2001**, *341*, 447.
(22) Hettich, R.; Lahamer, A.; Zhou, L.; Compton, R. *Int. J. Mass Spectrom.* **1999**, *183*, 335.
(23) Wang, S. Y.; Zhu, L.; Lu, J. Z.; Wang, P. N.; Li, Y. F. *Fullerene Sci. Technol.* **1994**, *2*, 49.
(24) Shinohara, H. *Rep. Prog. Phys.* **2000**, *63*, 843.
(25) Patchkovskii, S.; Thiel, W. *J. Am. Chem. Soc.* **1996**, *118*, 7164.
(26) *Fullerenes: Chemistry, Physics, and Technology*; Kadish, K. M., Rupff, R. S., Eds.; John Wiley & Sons: 2000; p 404.